J. Astrophys. Astr. (2018) 39:47
https://doi.org/10.1007/s12036-018-9542-5

Review

Prospects of detecting fast radio bursts using Indian radio telescopes

SIDDHARTHA BHATTACHARYYA

Department of Physics, Indian Institute of Technology Kharagpur, Kharagpur 721 302, India.
E-mail: siddhartha@phy.iitkgp.ac.in

MS received 10 May 2018; accepted 24 July 2018; published online 23 August 2018

Abstract. Fast Radio Bursts (FRBs) are short duration highly energetic dispersed radio pulses. We developed a generic formalism (Bera *et al.* 2016, MNRAS, 457, 2530) to estimate the FRB detection rate for any radio telescope with given parameters. By using this model, we estimated the FRB detection rate for two Indian radio telescope; the Ooty Wide Field Array (OWFA) (Bhattacharyya *et al.* 2017, J. Astrophys. Astr., 38, 17) and the upgraded Giant Metrewave Radio Telescope (uGMRT) (Bhattacharyya *et al.* 2018, J. Astrophys. Astr.) with three beam-forming modes. Here, we summarize these two works. We considered the energy spectrum of FRBs as a power law and the energy distribution of FRBs as a Dirac delta function and a Schechter luminosity function. We also considered two scattering models proposed by Bhat *et al.* (2004, Astrophys. J. Suppl. Series, 206, 1) and Macquart & Koay (2013, ApJ, 776, 125) for these works and we consider FRB pulse without scattering as a special case. We found that the future prospects of detecting FRBs by using these two Indian radio telescopes is good. They are capable to detect a significant number of FRBs per day. According to our prediction, we can detect $\sim 10^5-10^8$, $\sim 10^3-10^6$ and $\sim 10^5-10^7$ FRBs per day by using OWFA, commensal systems of GMRT and uGMRT respectively. Even a non detection of the predicted events will be very useful in constraining FRB properties.

Keywords. Cosmology—observations.

1. Introduction

Fast Radio Bursts (FRBs) are short duration ($\sim$ ms), highly energetic ($\sim 10^{32}-10^{34}$ J) dispersed radio pulses, first discovered (Lorimer *et al.* 2007) at the Parkes radio telescope. The high dispersion measure (DM) of the detected FRBs, which is in general $\sim$5–20 times excess DMs compared to what is expected from the Milky Way (Cordes & Lazio 2003), strongly suggests that FRBs are extragalactic events. The observed dispersion and the scattering indices imply the fact that the FRB signal propagates through the cold ionized plasma (Katz 2016) of the interstellar medium (ISM) of the Milky Way, host galaxy of the source and the intergalactic medium (IGM). A total of 35 FRBs have been reported[1] to date. Of these 26 FRBs have been detected at the Parkes radio telescope (Petroff *et al.* 2016, 2017; Keane *et al.* 2016; Ravi *et al.* 2016; Bhandari *et al.* 2017; Shannon *et al.* 2017; Price *et al.* 2018; Oslowski *et al.* 2018a, b), six FRBs have been detected at the UTMOST radio telescope (Caleb *et al.* 2017; Farah *et al.* 2017, 2018) and one each has been detected at the Arecibo (Spitler *et al.* 2014), GBT (Masui *et al.* 2015) and ASKAP (Bannister *et al.* 2017) radio telescopes. One FRBs has been found to repeat (Scholz *et al.* 2016) and 17 detections from the same source have been reported to date. There are several models (Kulkarni *et al.* 2015) proposed for the emission mechanism of FRBs but the exact one is still unknown. The energy spectrum and the energy distribution of FRBs are not well constrained and moreover the estimates of the spectral index of FRBs are available only for few FRBs but they are not reliably estimated due to the poor localization of the source within the single dish beam.

Bera *et al.* (2016) developed a generic formalism to estimate the detection rate and the redshift distribution of FRBs for a radio telescope with the given parameters. They assumed a power law $E_\nu \propto \nu^\alpha$ with α as the spectral index for the energy spectrum of FRBs and two scattering models proposed by Bhat *et al.* (2004) and Macquart & Koay (2013) for the predicted pulse width of FRBs and they are denoted here as

[1] http://frbcat.org/.

scattering model I (Sc-I) and II (Sc-II) respectively. Scattering model I (Sc-I) is an empirical fit to a large number of pulsar data in the Milky Way, whereas scattering model II (Sc-II) is purely theoretical without any observational consequences. The details of mathematical expression of scattering models I and II can be found in Bera *et al.* (2016). We also consider here FRB pulse without scattering as a special case, since for the most of the detected FRBs we did not find any scattering. The model is normalized by considering FRB 110220 as the reference event and the estimated energy ($E_0 = 5.4 \times 10^{33}$ J) of this FRB using our model as the reference energy. We also consider the prescribed FRB rate from Champion *et al.* (2016), i.e. 7×10^3 FRBs per sky per day as the reference event rate. Note that this prescribed FRB rate is differed from the FRB rate that was used in previous publications (Bera *et al.* 2016; Bhattacharyya *et al.* 2017, 2018) by a factor of $\sim 5 \times 10^5$. Note that, the value of E_0 is estimated by using the model prescribed in Bera *et al.* (2016) with $\alpha = -1.4$ ($E_\nu \propto \nu^\alpha$), which is differed from the energy mentioned in Thornton *et al.* (2013) by a factor of 5. As described in Bera *et al.* (2016), all redshifts are inferred from the DM; the scattering time scale, when available gives an upper limit on the redshift. We also considered two energy distribution functions: a Dirac delta function and a Schechter luminosity function with the exponent in the range $-2 \leq \gamma \leq 2$, as the possible energy distribution functions of FRBs.

Using the model mentioned above, we estimated the FRB detection rate for the two Indian radio telescopes, Ooty Wide Field Array (OWFA) (Bhattacharyya *et al.* 2017) and the upgraded Giant Metrewave Radio Telescope (uGMRT) (Bhattacharyya *et al.* 2018). We have found that the detection probability of FRBs largely depends on two factors: the field-of-view (FoV) of the telescope and the antenna sensitivity (A_S), where the antenna sensitivity is the ratio of the antenna gain (G) and the system temperature (T_{sys}) of the telescope. A telescope with large field-of-view (FoV) and high antenna sensitivity (A_S) is capable of detecting a large number of FRBs. Hence, the product FoV $\times$ A_S is a measure of the FRB detection sensitivity for a telescope. The typical value of this product for OWFA with the observational frequency of 326.5 MHz and uGMRT with the observational frequency of 375 MHz are 1.054 and 1.63×10^{-2} deg^2 Jy^{-1} respectively. However, this product is estimated by considering the higher galactic latitude (i.e., cold sky). For comparison, this value is 1.96×10^{-2} deg^2 Jy^{-1} for the Parkes telescope and 3.93×10^{-4} deg^2 Jy^{-1} for the Arecibo telescope. In this respect, both OWFA and uGMRT are capable of detecting a large number of FRBs in comparison to the Parkes and Arecibo radio telescopes.

This paper is a review of our previous works. Our predictions of FRB detection rates for OWFA and uGMRT are summarized. A brief outline of the paper is as follows. Section 2 presents a brief description and the FRB detection rates for OWFA. Section 3 presents a brief description and the FRB detection rates for GMRT and uGMRT. Section 4 presents FRB detection rate and localization comparison among OWFA, commensal systems of GMRT and uGMRT. Finally, the results are discussed and summarized in section 5.

2. Ooty Wide Field Array (OWFA)

The Ooty Wide Field Array (OWFA) is an upgraded version of the Ooty Radio Telescope (ORT) which was built in early 70s (Swarup *et al.* 1971) at Ooty, Tamil Nadu. ORT has a long cylindrical reflector of dimension 530 $\times$ 30 m,which contains 1056 half wavelength linear dipoles along the focal line of the reflector. The signal from the dipoles can be combined in different ways. Currently the signals from these dipoles are combined to form an analogue incoherent beam forming network which we refer to as the legacy system. The legacy system (LS) operates at an observational frequency $\nu_0 = 326.5$ MHz ($\lambda = 0.91$ m) with bandwidth $B = 4$ MHz. The system is being upgraded to two modes of operation: Phase I (PI) and Phase II (PII). In Phase I, 24 dipoles are combined together to form a single element and this system has a total 40 such elements. In Phase II, 4 dipoles are combined together to form a single element and this system has a total 264 such elements. The bandwidth of Phase I and Phase II are 19.2 MHz and 38.4 MHz respectively, centred at the same observational frequency of the ORT Legacy System. More technical information about OWFA can be found in Subrahmanya *et al.* (2017). The system specifications of LS, PI and PII are tabulated in Table 1.

In this work, we considered three kinds of beam formations: incoherent (IA), coherent single (CA-SB) and coherent multiple (CA-MB) beam formations. In the case of incoherent beam formation (IA), the squares of the voltages from the individual elements are summed over to obtain the total power. This mode of beam formation does not contain any phase information. Here the FoV is proportional to λ/d, where d is the length of a single element. The sensitivity in this mode is increased by a factor of $\sqrt{N_A}$ compared to the sensitivity achieved

Table 1. The number of FRBs expected to be detected per day by considering the Dirac delta function as the energy distribution function of FRBs and the mean value of α with error for the range $-5 \leq \alpha \leq 0$, where $E_\nu \propto \nu^\alpha$. Two scattering models and FRB signal without scattering have been considered for the detection rate comparison. Here IA, CA-SB, CA-MB and MIA denote incoherent, coherent single beam, coherent multiple beam and multiple incoherent beam formations respectively. The symbols ν, B, $F_{\rm th}$ and FoV denote observational frequency of the telescope, bandwidth of the observation, threshold fluence of FRB required for the detection and the field-of-view of the telescope respectively.

		ν	B	Beam	$F_{\rm th}$	FoV	FRB detection rate (day^{-1})		
Telescope	System	(MHz)	(MHz)	formation	(Jy ms)	(deg^2)	Scattering Model I	Scattering Model II	Without scattering
OWFA	LS	326.5	4	IA	6.88	0.52	$(2.37 \pm 1.09) \times 10^5$	$(1.17 \pm 0.64) \times 10^6$	$(2.11 \pm 0.23) \times 10^6$
	PI			IA	22.80	24.11	$(7.19 \pm 1.29) \times 10^6$	$(3.34 \pm 0.91) \times 10^7$	$(8.95 \pm 0.32) \times 10^7$
		326.5	19.2	CA-SB	3.61	0.60	$(3.43 \pm 0.98) \times 10^5$	$(1.68 \pm 0.53) \times 10^6$	$(3.12 \pm 0.10) \times 10^6$
				CA-MB	1.08	24.11	$(1.92 \pm 0.82) \times 10^7$	$(8.93 \pm 0.31) \times 10^7$	$(1.38 \pm 0.13) \times 10^8$
	PII			IA	38.10	143.34	$(3.55 \pm 1.42) \times 10^7$	$(1.61 \pm 1.03) \times 10^8$	$(4.33 \pm 0.48) \times 10^8$
		326.5	38.4	CA-SB	2.34	0.55	$(3.49 \pm 0.92) \times 10^5$	$(1.69 \pm 0.45) \times 10^6$	$(2.80 \pm 0.10) \times 10^6$
				CA-MB	0.70	143.34	$(1.29 \pm 0.77) \times 10^8$	$(5.77 \pm 0.22) \times 10^8$	$(8.26 \pm 0.13) \times 10^8$
GMRT	Band S1			IA	2.25	1.62	$(3.60 \pm 0.95) \times 10^5$	$(1.73 \pm 0.48) \times 10^6$	$(2.93 \pm 0.10) \times 10^6$
		300	32	CA-SB	0.41	5.25×10^{-6}	$(5.71 \pm 0.74) \times 10^3$	$(2.44 \pm 0.16) \times 10^4$	$(3.32 \pm 0.10) \times 10^4$
				MIA	1.17	1.62	$(4.32 \pm 0.87) \times 10^5$	$(2.02 \pm 0.37) \times 10^6$	$(3.12 \pm 0.12) \times 10^6$
	Band S2			IA	2.25	0.72	$(4.12 \pm 0.73) \times 10^4$	$(2.00 \pm 0.27) \times 10^5$	$(3.41 \pm 0.20) \times 10^5$
		450	32	CA-SB	0.41	2.33×10^{-6}	$(3.59 \pm 0.55) \times 10^3$	$(1.57 \pm 0.10) \times 10^4$	$(2.15 \pm 0.13) \times 10^4$
				MIA	1.17	0.72	$(5.01 \pm 0.66) \times 10^4$	$(2.38 \pm 0.12) \times 10^5$	$(3.67 \pm 0.18) \times 10^5$
uGMRT	Band 2			IA	5.21	4.26	$(5.19 \pm 1.46) \times 10^5$	$(2.52 \pm 0.77) \times 10^6$	$(4.27 \pm 0.41) \times 10^6$
		185	130	CA-SB	0.95	1.38×10^{-5}	$(8.35 \pm 1.12) \times 10^3$	$(3.67 \pm 0.52) \times 10^4$	$(5.06 \pm 0.09) \times 10^4$
				MIA	2.71	4.26	$(6.32 \pm 1.31) \times 10^5$	$(2.99 \pm 0.66) \times 10^6$	$(4.64 \pm 0.29) \times 10^6$
	Band 3			IA	0.90	1.04	$(3.79 \pm 0.78) \times 10^6$	$(1.73 \pm 0.22) \times 10^7$	$(2.30 \pm 0.12) \times 10^7$
		375	250	CA-SB	0.16	3.36×10^{-6}	$(5.83 \pm 0.59) \times 10^3$	$(2.24 \pm 0.11) \times 10^4$	$(2.63 \pm 0.10) \times 10^4$
				MIA	0.47	1.04	$(4.52 \pm 0.70) \times 10^6$	$(1.95 \pm 0.08) \times 10^7$	$(2.46 \pm 0.14) \times 10^7$
	Band 4			IA	0.69	0.30	$(1.94 \pm 0.37) \times 10^5$	$(9.01 \pm 0.31) \times 10^5$	$(1.15 \pm 0.28) \times 10^6$
		700	300	CA-SB	0.13	9.64×10^{-7}	$(2.94 \pm 0.24) \times 10^3$	$(1.17 \pm 0.26) \times 10^4$	$(1.35 \pm 0.18) \times 10^4$
				MIA	0.36	0.30	$(2.31 \pm 0.32) \times 10^5$	$(1.02 \pm 0.35) \times 10^6$	$(1.25 \pm 0.23) \times 10^6$
	Band 5			IA	0.63	0.09	$(1.85 \pm 0.03) \times 10^4$	$(8.82 \pm 0.60) \times 10^4$	$(1.05 \pm 0.45) \times 10^5$
		1250	400	CA-SB	0.12	3.02×10^{-7}	$(1.55 \pm 0.13) \times 10^3$	$(6.34 \pm 0.36) \times 10^3$	$(7.04 \pm 0.29) \times 10^3$
				MIA	0.33	0.09	$(2.23 \pm 0.07) \times 10^4$	$(1.01 \pm 0.49) \times 10^5$	$(1.16 \pm 0.37) \times 10^5$
CHIME				IA	5.80	132.00	$(1.79 \pm 0.82) \times 10^8$	$(8.93 \pm 0.32) \times 10^8$	$(1.17 \pm 0.11) \times 10^9$
	–	600	400	CA-SB	0.16	0.29	$(1.10 \pm 0.37) \times 10^6$	$(4.36 \pm 0.24) \times 10^6$	$(4.83 \pm 0.18) \times 10^6$

by a single element. Note that LS operates with incoherent beam forming mode. In the case of coherent single beam formation (CA-SB), the voltage signals from the individual elements with phase are added directly and then squared to obtain total power. In this mode, the field-of-view (FoV) is proportional to λ/D, where λ is the wavelength of the observation and D is the length of the largest baseline. Here the sensitivity is increased by a factor of $N_{\rm A}$ compared to the sensitivity achieved by a single element. The coherent multiple beam formation is a mixture of IA and CA-SB mentioned above. In coherent multiple beam formation (CA-MB), one forms the IA to obtain a large instantaneous field-of-view but at a relatively shallow sensitivity. When an event is detected in the IA mode, the high time resolution signals are recorded to eventually form multiple coherent beams-offline in all possible directions. This will give us the sensitivity of the CA-SB, but with the field-of-view of the IA and hence the detection probability in this mode is larger than the same for IA and CA-SB modes. This specific kind of strategy was first demonstrated in a pilot transient survey with the Giant Metrewave Radio Telescope (GMRT) by Bhat *et al.* (2013). Note that the value of threshold signal-to-noise ratio ($(S/N)_{\rm th}$) for this beam-forming mode is less when compared to the same for IA and CA-SB modes. In this work, $(S/N)_{\rm th} = 3$ for CA-MB mode and $(S/N)_{\rm th} = 10$ for IA and CA-SB beam forming modes.

We considered the energy spectrum of FRBs as $E_\nu \propto \nu^\alpha$ for this work and α is defined here as the spectral index. We estimated the FRBs detection rates for ORT-legacy system, OWFA Phase I and II and compared the results with other two cylindrical radio telescopes, UTMOST (Caleb *et al.* 2016) and CHIME (Newburgh *et al.* 2014). Note that UTMOST operates at an observational frequency of 843 MHz with a bandwidth of 31.25 MHz, whereas CHIME operates at an observational frequency of 600 MHz with a bandwidth of 400 MHz. Figure 1 shows the FRB detection rates as a function of α for OWFA Phase I and Phase II, UTMOST and CHIME with three beam forming modes IA, CA-SB and CA-MB and the ORT legacy system. It is found that the detection rate varies with different scattering models and the detection rate is maximum for the case of FRB pulse without scattering, which is roughly two order and one order of magnitude larger than the same for scattering models I and II respectively. Further the detection rate increases with decreasing α ($\alpha \leq 0$). In brief, we expect to detect $\sim 10^5 - 10^8$ FRBs per day by using OWFA Phase II with fluence $F \geq 0.7$ Jy ms, which is also large when compared to that for UTMOST.

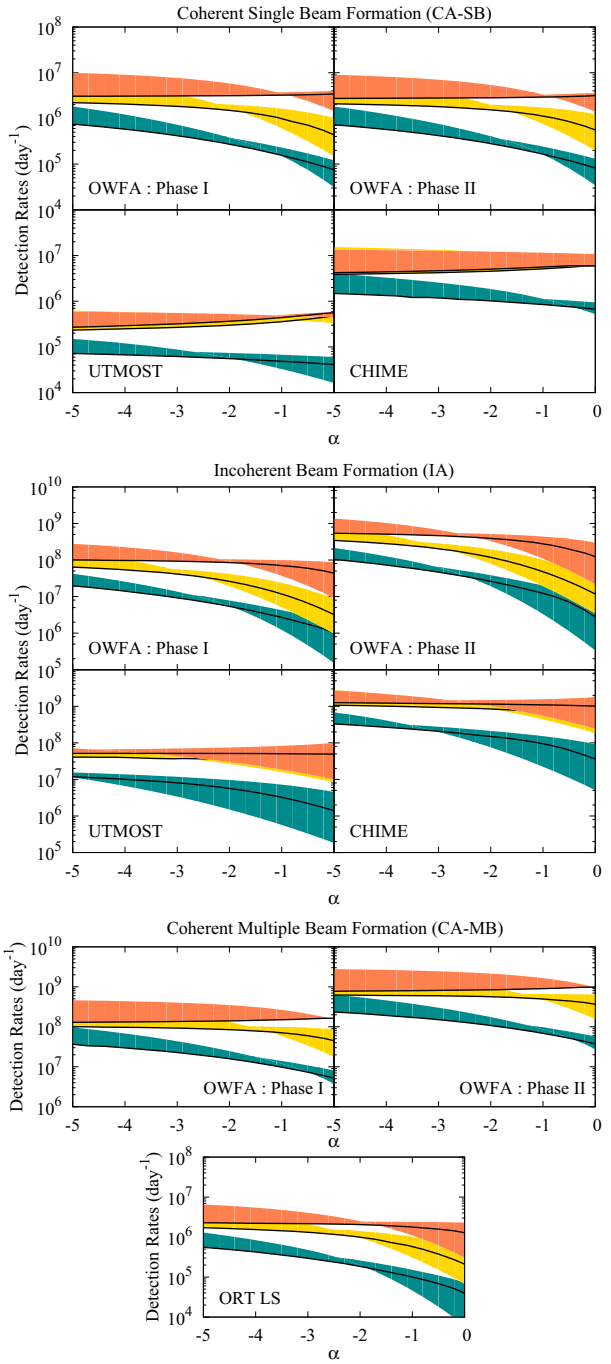

Figure 1. The variation of the FRB detection rate with the variation of α, where $E_\nu \propto \nu^\alpha$ for ORT legacy system, OWFA Phase I and Phase II, UTMOST and CHIME with three kinds of beam formations: IA, CA-SB and CA-MB. Two scattering models Sc-I (green region) and Sc-II (yellow region) and FRB pulse without scattering (orange region) have been considered here. The solid black lines denote the Dirac delta function, while the boundaries of the regions enclosing the curves correspond to the Schechter luminosity function with an exponent in the range $-2 \leq \gamma \leq 2$.

However, the detection rate is maximum for the CHIME due to its large field-of-view but these three telescopes operate in different frequency ranges and hence complementary.

3. Upgraded Giant Metrewave Radio Telescope (uGMRT)

The GMRT antennas are distributed in a Y-shaped pattern with a shortest baseline of 200 m and a longest baseline of 25 km. Each dish has five prime focus feeds, only one of which is available at a given time, having five discrete operational frequencies centered at 150, 235, 325, 610 and 1280 MHz with a maximum backend instantaneous frequency bandwidth of 32 MHz. Currently the GMRT is going through an upgradation (Gupta *et al.* 2017), to provide significantly large instantaneous bandwidths with four operational frequencies, viz., Band 2 at 185 MHz with a bandwidth of 130 MHz, Band 3 at 375 MHz with a bandwidth of 250 MHz, Band 4 at 700 MHz with a bandwidth of 300 MHz and Band 5 at 1250 MHz with a bandwidth of 400 MHz.

In this work, we also considered the proposed commensal system for the GMRT (Bhattacharyya *et al.* 2018). This system as currently envisaged, would reuse the legacy signal transport chain of the GMRT, which has a bandwidth of 32 MHz. The feed system is proposed to be mounted off-focus on the quadripod feed legs of the GMRT, and hence will be available at all times, unlike the main feeds, which are mounted on a rotating turret, and of which only one feed is available at a given time. We examined the expected detection rate for two possible central frequencies, viz. 300 and 450 MHz with a bandwidth of 32 MHz, which roughly span the possible frequencies of the proposed system and they are denoted here as Bands S1 and S2 respectively. In both the GMRT commensal systems and uGMRT, we considered three kinds of beam formations: incoherent (IA), coherent single (CA-SB) and multiple incoherent (MIA) beam formations. The description of IA and CA-SB have been mentioned earlier and MIA mode is a special beam-forming mode for the both the commensal systems of GMRT and the four frequency bands of uGMRT.

In the MIA beam-forming mode, the entire array is divided into multiple ($N_{\rm Array}$) sub-arrays each of which operates in the IA mode. This will give us the large field-of-view of the IA with shallow sensitivity compared to IA. A signal is considered as an event if and only if it is detected in all the sub arrays. In practice, because the co-incidence filtering greatly reduces false alarms (Bhat *et al.* 2013), one can use a lower signal-to-noise ratio threshold $(\mathrm{S/N})_{\rm th}$ ($\geq$3) for each sub-array. Although the MIA mode has a lower sensitivity compared to the IA mode, the reduced detection threshold more than compensates for this and we found a higher FRB detection rate for the MIA mode as compared to the IA mode. Note that in this work, we considered $(\mathrm{S/N})_{\rm th} = 3$ and $N_{\rm Array} = 3$ for the MIA beam forming mode. The system specifications of two commensal systems of GMRT and four frequency bands of uGMRT are tabulated in Table 1.

Figure 2 shows the variation of FRB detection rates with the variation of α for the commensal systems of GMRT and the four frequency bands of uGMRT with three beam-forming modes (IA, CA-SB and MIA). As mentioned earlier, it is also found here that the detection rate varies with different scattering models and the detection rate is maximum for the case of FRB pulse without scattering, which is roughly $\sim$10 and $\sim$2 times larger than the same for scattering models I and II respectively. Further it also increases with decreasing α. In a brief, we expect to detect $\sim 10^3 - 10^6$ FRBs per day with fluence $F \geq 0.41$ Jy ms for the commensal system of GMRT and $\sim 10^5 - 10^7$ FRBs per day with fluence $F \geq 0.12$ Jy ms for the four frequency bands of uGMRT respectively.

4. FRB detection rate and localization comparison

In this section, we compare FRB detection rate and localization of the event for the three phases of OWFA (LS, PI and PII), the two commensal systems of GMRT (Bands S1 and S2), the four observational frequency bands of uGMRT (Bands 2, 3, 4 and 5) and CHIME. Table 1 shows the number of FRBs expected to be detected per day by considering the Dirac delta function as the energy distribution function of FRBs and the mean value of α with error for the range $-5 \leq \alpha \leq 0$, where $E_\nu \propto \nu^\alpha$, for different systems of OWFA, GMRT, uGMRT and CHIME with their observational frequency, bandwidth, beam formations, field of view and threshold fluence of the event required for the detection. It is found that the detection rate is larger for FRB pulse without scattering than the same for scattering models I and II respectively. In Table 1, the detection rate is large ($\sim 8.26 \times 10^8$ FRBs per day) for OWFA Phase II with CA-MB beam forming mode in comparison to the commensal systems of GMRT and uGMRT, but the detection rate is maximum ($\sim 1.17 \times 10^9$ FRBs per day) for CHIME with IA beam forming mode. However, OWFA and the commensal systems of GMRT,

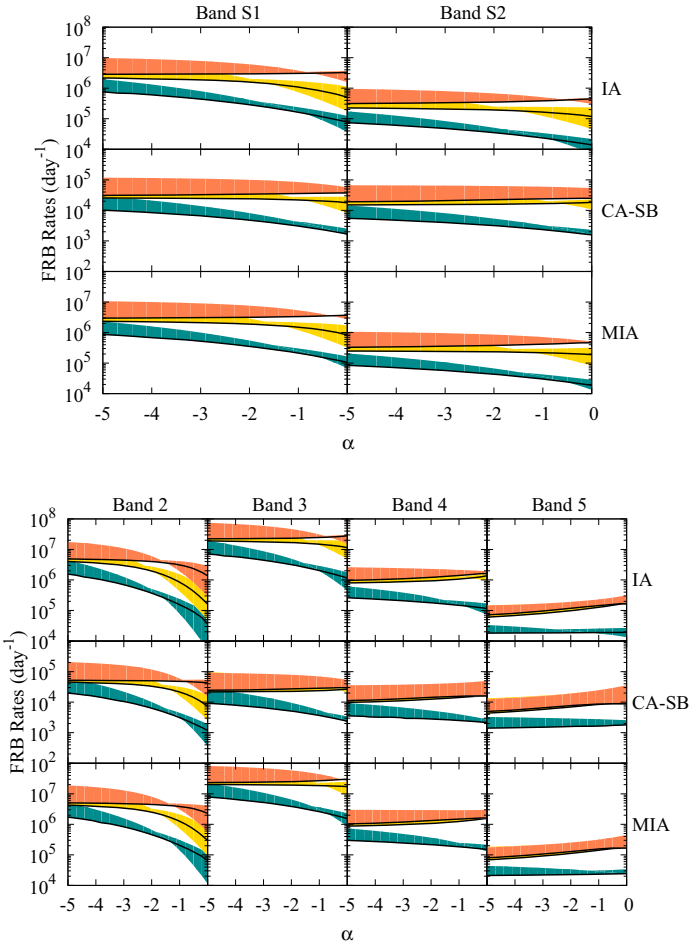

Figure 2. The variation of the FRB detection rate with the variation of α for the proposed commesal system of GMRT and the four frequency bands of uGMRT with three kinds of beam formations: IA, CA-SB and MIA. Two scattering models Sc-I (green region) and Sc-II (yellow region) and the FRB pulse without scattering (orange region) have been considered here. The solid black lines denote the Dirac delta function, while the boundaries of the regions enclosing the curves correspond to the Schechter luminosity function with an exponent in the range $-2 \leq \gamma \leq 2$.

uGMRT and CHIME operate in different frequency ranges and hence complementary.

The quantity $F_{\rm th}$ is an important parameter of FRB detection. We can detect a FRB if and only if the fluence of this event is larger than the value of $F_{\rm th}$ for a given radio telescope. For OWFA, it is found that we can detect bright FRBs by using the IA beam-forming mode, whereas CA-MB mode can be used to detect a variety of FRBs. Similarly for the two commensal systems of GMRT and the four frequency bands of uGMRT, we can detect a variety of FRBs by using MIA beam forming mode, whereas IA mode can be used to detect only bright FRBs. In contrast, CHIME can only detect bright FRBs.

The localization of the event depends on the field-of-view (FoV) of the telescope. A telescope with large field-of-view can localize an event poorly in comparison to the same for a telescope with small field-of-view. From Table 1, it is found that the localization of FRBs is much better for the two commensal systems of GMRT and the four frequency bands of uGMRT with CA-SB beam forming mode in comparison to others. The localization of the event is much poorer for OWFA, where the dipoles are aligned along the focal line of the cylindrical reflector and hence it can only localize the event along a straight line in the North–South direction. However as mentioned earlier, the detection probability of FRBs largely depend on the product of field-of-view and sensitivity of the telescope and hence OWFA is capable to detect a large number of FRBs in comparison to the same for others mentioned in Table 1. In brief, we can detect a large number of FRBs with poor localization by using OWFA, whereas the two commensal systems of GMRT and the four frequency bands of uGMRT can

be used to detect a comparatively less number of FRBs with better localization. For CHIME, the localization of detected FRBs (field-of-view $= 132$ deg^2) is quite poor in comparison to OWFA, the commensal systems of GMRT and uGMRT.

5. Summary and conclusion

Fast Radio Bursts (FRBs) are short duration highly energetic dispersed radio pulses. Here we have summarized our predictions of detecting FRBs using OWFA (Bhattacharyya *et al.* 2017) and uGMRT (Bhattacharyya *et al.* 2018) with different beam forming modes. We used the model prescribed by Bera *et al.* (2016) for those predictions. We considered the energy spectrum of FRBs as a power law and the energy distribution of FRBs as a Dirac delta function and Schechter luminosity function with both positive and negative exponents. We also considered two scattering models prescribed by Bhat *et al.* (2004) and Macquart & Koay (2013) and FRB pulse without scattering as a special case for the prediction of FRB pulse width.

We have first discussed our predictions of FRB detection rate for the Ooty Wide Field Array (OWFA). OWFA is an upgraded version of the Ooty Radio Telescope (ORT). ORT has a long cylindrical reflector of dimension 530×30 m,which contains 1056 half wavelength linear dipoles along the focal line of the reflector. The signals from these dipoles are combined in a different way and we have discussed our predictions for the old analogue beam-forming network, legacy system, and the upcoming Phase I and Phase II and compared the results with UTMOST and CHIME. In this work, we considered three kinds of beam formations: incoherent (IA), coherent single (CA-SB) and coherent multiple (CA-MB) beam formations. We found that we can expect to detect $\sim 10^5 - 10^8$ FRBs per day by using OWFA with a fluence of $F \geq 0.7$ Jy ms.

We next discussed our predictions of FRB detection rate for the upgraded Giant Metrewave Radio Telescope (uGMRT) with three kinds of beam formations: incoherent (IA), coherent single (CA-SB) and multiple incoherent (MIA) beam formations. The uGMRT is an upgraded version of the GMRT, which has 30 parabolic dishes having 45 m diameter each and they are distributed in a Y-shaped pattern with a shortest baseline of 200 m and a longest baseline of 25 km. Each dish has five prime focus feeds having five discrete operational frequencies centered at 150, 235, 325, 610 and 1280 MHz with a maximum backend instantaneous frequency bandwidth of 32 MHz. uGMRT will provide significantly large instantaneous bandwidths with four operational frequencies centered at 185, 375, 700 and 1250 MHz with a wide variation of bandwidths from 130 to 400 MHz. In this work, we also considered the proposed commensal system for the GMRT for transient search. We found that we expect to detect $\sim 10^3 - 10^6$ FRBs per day with fluence $F \geq 0.41$ Jy ms for the commensal system of GMRT and $\sim 10^5 - 10^7$ FRBs per day with fluence $F \geq 0.12$ Jy ms for the four frequency bands of uGMRT respectively. Further it is found that OWFA and the lower frequency bands of GMRT and uGMRT can detect bright FRBs only, whereas the higher frequency bands of GMRT and uGMRT can be used to detect a variety of FRBs. It is also found that we can detect a large number of FRBs with poor localization by using OWFA, whereas the two commensal systems of GMRT and the four frequency bands of uGMRT can be used to detect a comparatively less number of FRBs with better localization.

However, there are some uncertainties and limitations in our predictions. The scattering mechanism in the intervening medium is still unknown. Further, there is no unique and direct way to estimate the spectral index of FRBs. Moreover, the energy distribution function of FRBs is another important unknown quantity, and we have considered two possible energy distribution models in this analysis. The detection of a large number of FRBs in future will help us to constrain these uncertainties and refine the FRBs models.

References

Bannister K. W. *et al*. 2017, ApJL, 841, L12
Bera A. *et al*. 2016, MNRAS, 457, 2530
Bhandari S. *et al*. 2017, ArXiv e-prints: arXiv:1711.08110
Bhat N. D. R., Cordes J. M. *et al*. 2004, ApJ, 605, 759
Bhat N. D. R. *et al*. 2013, Astrophys. J. Suppl. Series, 206, 1
Bhattacharyya S. *et al*. 2017, J. Astrophys. Astr., 38, 17
Bhattacharyya S. *et al*. 2018, J. Astrophys. Astr., submitted
Caleb M. *et al*. 2016, MNRAS, 458, 718
Caleb M. *et al*. 2017, MNRAS, 468, 3746
Champion D. J. *et al*. 2016, MNRAS, 460, L30
Cordes J. M., Lazio T. J. W. 2003, ArXiv eprint: arXiv:astro-ph/0207156
Farah W. *et al*. 2017, The Astronomer's Telegram, 10697
Farah W. *et al*. 2018, The Astronomer's Telegram, 11675
Gupta Y. *et al*. 2017, Curr. Sci., 113, 4
Katz J. I. 2016, Mod. Phys. Lett. A, 31, 14
Keane E. F. *et al.* 2016, Nature, 530, 453
Kulkarni S. R. *et al*. 2015, ArXiv e-prints: arXiv:1511.09137
Lorimer D. R. *et al*. 2007, Science, 318, 777
Macquart J. P., Koay J. Y. 2013, ApJ, 776, 125
Masui K. *et al*. 2015, Nature, 528, 523

Newburgh L. B. *et al*. 2014, SPIE Proc., 9145
Oslowski S. *et al*. 2018a, The Astronomer's Telegram, 11396
Oslowski S. *et al*. 2018b, The Astronomer's Telegram, 11851
Petroff E. *et al*. 2016, PASA, 33
Petroff E. *et al*. 2017, MNRAS, 469, 4465
Price D. C. *et al*. 2018, The Astronomer's Telegram, 11376
Ravi V. *et al*. 2016, Science, https://doi.org/10.1126/science.aaf6807
Scholz P. *et al*. 2016, ApJ, 833, 177
Shannon R. M. *et al*. 2017, The Astronomer's Telegram, 11046
Spitler L. G. *et al*. 2014, ApJ, 790, 101
Subrahmanya C. R. et al. 2017, J. Astrophys. Astr., 38, 10
Swarup G., Sarma N. V. G. *et al*. 1971, Nat. Phys. Sci., 230, 185
Thornton D. *et al*. 2013, Science, 341, 53